FROM ZO TO CO WITH DIFFRACTIONS: THEORY

A. Bauer, B. Schwarz, and D. Gajewski

email: *alex.bauer@uni-hamburg.de*
keywords: *common-offset, CRS, diffractions, stacking*

ABSTRACT

As it leads to a first interpretable time image, the simulation of a zero-offset section is still one of the key processing steps in seismic imaging. The zero-offset approximations are reasonably accurate, when lateral heterogeneity is moderate. Recent works indicate that common-offset stacking improves resolution and illumination in complex settings, which become increasingly important in exploration. However, due to the higher dimensionality of the problem, common-offset stacking is computationally more expensive. In this work, we motivate a straightforward decomposition principle for diffractions, which establishes a direct connection between zero-offset and common-offset diffraction wavefield attributes based on the decoupling of diffraction raypaths. We show, theoretically and by fitting traveltimes, that each common-offset diffraction operator can be decomposed exactly into two zero-offset operators. This allows the direct prediction of common-offset diffraction attributes from the zero-offset section. Application of the new method to simple waveform data reveals its ability to reliably image diffractions solely based on zero-offset measurements.

INTRODUCTION

Being an extension of the classical common-midpoint (CMP) stack, multi-parameter stacking is an important tool in seismic imaging. The 2D common reflection surface (CRS) stack is such a multi-parameter approach, in which stacking is not only carried out along a traveltime moveout curve in offset direction, but along a traveltime moveout surface in both offset and midpoint direction. CRS processing is purely data-driven and provides stacked sections with significantly increased signal-to-noise ratio compared to the CMP stack. This is required particularly in areas with complex geology and sparse illumination.

The CRS stack has been formulated for a central zero-offset (ZO) ray (Jäger et al., 2001) and for an arbitrary common-offset (CO) central ray (Zhang et al., 2001). While the widely used ZO CRS stack is fast and reasonably accurate for moderate lateral heterogeneity, CO CRS shows its strengths in complex geological settings, where it provides improved resolution and illumination at the cost of being computationally more expensive (see, e.g., Spinner et al., 2012).

For the computation of traveltime moveout around the central ray, the CRS stack uses a hyperbolic second-order approximation. The 2D ZO approximation is parametrized by three kinematic wavefield attributes (Hubral, 1983). The CO CRS stack (Zhang et al., 2001) generalizes this parametrization to arbitrary source and receiver combinations and thus can characterize the full pre-stack data volume. Since up- and downgoing raypaths do not coincide in the CO case, the CO traveltime approximation includes five wavefield attributes, which results in a higher dimensionality of the problem. In the diffraction case, however, moveouts in the common-shot (CS) and the common-receiver (CR) gather are decoupled and as a result, ZO and CO information is highly redundant for diffractions (Schwarz et al., 2014; Bauer, 2014).

Recent works indicate that CO processing may be based on ZO operators, when the degree of complexity is relatively low (see, e.g., Baykulov and Gajewski, 2009). Baykulov and Gajewski (2009) introduced a ZO-based partial CRS stacking scheme, which simulates CO sections by the global application of ZO operators. This method is computationally very efficient, but loses accuracy for higher offsets and in complex

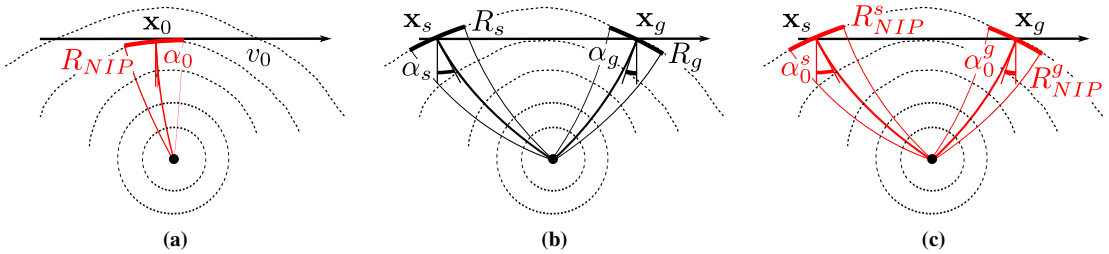

Figure 1: The two common-offset NIP-wave experiments (b) may be resembled by two indepent zero-offset NIP-wave experiments (c) at a source $\mathbf{x}_s$ and a receiver $\mathbf{x}_g$.

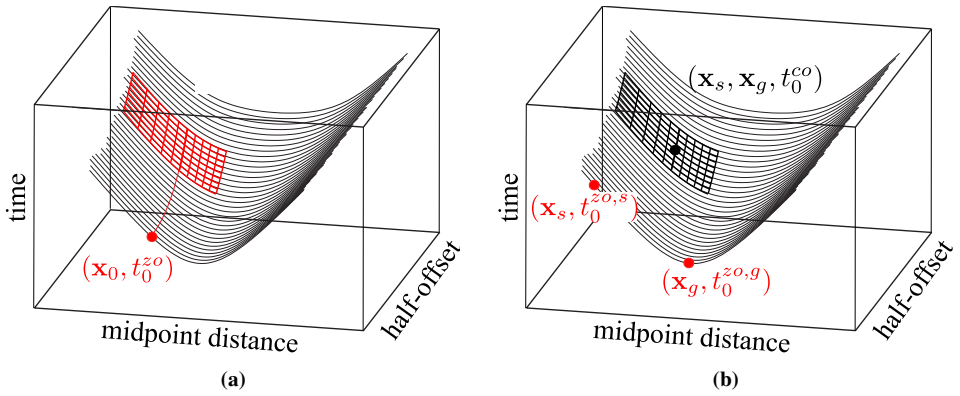

Figure 2: The partial CRS stacking surface (a) is based on extrapolation of ZO operators. The CO prediction stacking surface is based on a CO operator, which is constructed by two ZO diffraction operators at a source $\mathbf{x}_s$ and a receiver $\mathbf{x}_g$.

settings. The generic CO stack, however, is accurate for arbitrary offsets and in complex settings.

In this work, we motivate a method which makes use of the redundancy of ZO and CO information for diffractions using the results of ZO CRS processing as a starting point for CO diffraction stacking. We show theoretically, by fitting traveltimes for a simple heterogeneous model and on simple waveform data that each CO diffraction operator can be decomposed exactly into two ZO operators, which allows the direct prediction of CO diffraction attributes based on ZO results. All results presented in this work are compared to the ones obtained from the ZO-based partial CRS method (Baykulov and Gajewski, 2009) and generic CO CRS processing (Zhang et al., 2001).

THEORY

Zero-offset CRS stack

In the reflection case, the zero-offset CRS traveltime moveout depends on three parameters, the kinematic wavefield attributes α_0, R_{NIP} and R_{N} (Hubral, 1983). The latter ones, R_{NIP} and R_{N}, describe the radii of two ficticious wavefronts, the NIP-wave and the normal wave. While the NIP-wave stems from a ficticious point source placed on the reflector's point of normal incidence (NIP), the normal wave is emitted by a ficticious exploding reflector segment around the NIP. The angle α_0 describes the direction out of which the two ficticious waves emerge at the central midpoint. For the computation of the CRS traveltime, different traveltime formulations exist. In this work, the hyerbolic and the parabolic traveltime descriptions are used. The hyperbolic CRS traveltime (Müller, 1999) reads

$$t^2_{\mathrm{ZO}}(\Delta\mathbf{x}_m, \mathbf{h}) = \left(t_0^{\mathrm{ZO}} + \frac{2\sin\alpha_0}{v_0}\Delta\mathbf{x}_m\right)^2 + \frac{2t_0\cos^2\alpha_0}{v_0}\left(\frac{\Delta\mathbf{x}_m^2}{R_{\mathrm{N}}} + \frac{\mathbf{h}^2}{R_{\mathrm{NIP}}}\right), \tag{1}$$

where $\Delta\mathbf{x}_m = \mathbf{x}_m - \mathbf{x}_0$ is the displacement from the central midpoint $\mathbf{x}_0$, $\mathbf{h}$ denotes the half-offset and v_0 the constant near-surface velocity. The parabolic CRS traveltime (Müller, 1999) reads

$$t_{\text{ZO}}(\Delta\mathbf{x}_m, \mathbf{h}) = t_0^{\text{ZO}} + \frac{2\sin\alpha_0}{v_0}\Delta\mathbf{x}_m + \frac{\cos^2\alpha_0}{v_0 R_{\text{NIP}}}\mathbf{h}^2 + \frac{\cos^2\alpha_0}{v_0 R_{\text{N}}}\Delta\mathbf{x}_m^2. \tag{2}$$

In the special case of a diffraction this traveltime moveout only depends on two parameters, because the NIP-wave and the normal wave coincide,

$$t_{\text{ZO}}(\Delta\mathbf{x}_m, \mathbf{h}) = t_0^{\text{ZO}} + \frac{2\sin\alpha_0}{v_0}\Delta\mathbf{x}_m + \frac{\cos^2\alpha_0}{v_0 R_{\text{NIP}}}\left(\Delta\mathbf{x}_m^2 + \mathbf{h}^2\right). \tag{3}$$

As illustrated in Figure 1(a), the NIP-wave approximates the actual physical wavefront in the ZO section ($\mathbf{h} = 0$),

$$t_{\text{ZO}}(\Delta\mathbf{x}_m) = t_0^{\text{ZO}} + \frac{2\sin\alpha_0}{v_0}\Delta\mathbf{x}_m + \frac{\cos^2\alpha_0}{v_0 R_{\text{NIP}}}\Delta\mathbf{x}_m^2. \tag{4}$$

Based on the ZO CRS stack, Baykulov and Gajewski (2009) recently introduced the so-called partial CRS stack. In this method, common-offset traces are simulated by global application of zero-offset operators. Figure 2(a) shows an example of a partial CRS stacking surface. The expansion point of the zero-offset operator is marked in red. Due to the smaller number of parameters this method is computationally more efficient than the generic common-offset stack and in cases of moderate complexity and for small partial stacking apertures zero-offset operators perform reasonably well. However, the zero-offset approximation loses accuracy with increasing offsets and complexity. Therefore, we argue that common-offset operators should be used for local refinement at far offsets (see also Bauer (2014); Schwarz et al. (2014)). In the following, the partial CRS method will be referred to as *common-offset extrapolation*.

Common-offset CRS stack

The common-offset CRS stack (Zhang et al., 2001) is a generalization of the zero-offset CRS stack to arbitrary source and receiver combinations, which allows the simulation of the full pre-stack data volume. Due to the higher dimensionality of the problem the CO CRS stack cannot be parametrized by only three parameters. Instead, because of the asymmetry of up- and downgoing raypaths, the CO CRS parameters describe the attributes of the respective two-way wavefronts and a coupling coefficient. The five-parameter hyperbolic CO CRS traveltime in source ($\mathbf{x}_s = \mathbf{x}_m - \mathbf{h}$) and receiver ($\mathbf{x}_g = \mathbf{x}_m + \mathbf{h}$) coordinates (Bergler et al., 2002) is given by

$$\begin{aligned} t_{\text{CO}}^2(\Delta\mathbf{x}_s, \Delta\mathbf{x}_g) = &\left(t_0^{\text{CO}} + \frac{\sin\alpha_s}{v_s}\Delta\mathbf{x}_s + \frac{\sin\alpha_g}{v_g}\Delta\mathbf{x}_g\right)^2 \\ &+ 2t_0^{\text{CO}}\left(\frac{1}{2}B^{-1}A\Delta\mathbf{x}_s^2 + \frac{1}{2}DB^{-1}\Delta\mathbf{x}_g^2 + B^{-1}\Delta\mathbf{x}_s\Delta\mathbf{x}_g\right), \end{aligned} \tag{5}$$

where $\Delta\mathbf{x}_s$ and $\Delta\mathbf{x}_g$ denote the displacements from the central source $\mathbf{x}_s$ and receiver $\mathbf{x}_g$, respectively. Further, the angles of emergence at source and receiver are denoted by α_s and α_g and accordingly, v_s and v_g are the near surface velocities. The quantities A, B and D are the scalar elements of the surface-to-surface ray propagator matrix introduced by Bortfeld (1989). Zhang et al. (2001) describe these quantities in terms of the two emergence angles and three wavefront curvatures, which correspond to ficticious two-way waves observed in the common-shot (CS) and common-midpoint (CMP) configurations.

As it follows from a direct expansion of the traveltime, the parabolic common-offset CRS traveltime formulation is physically more intuitive than its hyperbolic counterpart. It reads

$$\begin{aligned} t_{\text{CO}}(\Delta\mathbf{x}_s, \Delta\mathbf{x}_g) = t_0^{\text{CO}} &+ \frac{\sin\alpha_s}{v_s}\Delta\mathbf{x}_s + \frac{1}{2}\frac{\cos^2\alpha_s}{v_s R_s}\Delta\mathbf{x}_s^2 \\ &+ \frac{\sin\alpha_g}{v_g}\Delta\mathbf{x}_g + \frac{1}{2}\frac{\cos^2\alpha_g}{v_g R_g}\Delta\mathbf{x}_g^2 \\ &+ B^{-1}\Delta\mathbf{x}_s\Delta\mathbf{x}_g, \end{aligned} \tag{6}$$

The coefficients of this second-order expression are parametrized by the emergence angles α_s, α_g and the radii of curvature R_s, R_g of the wavefronts measured in the common-shot (CS) and common-receiver (CR) configurations, respectively. The matrix element B^{-1} couples the moveouts in the CS and CR gathers. In the diffraction case the coupling between the two-way wavefronts vanishes and they reduce to one-way waves (see Figure 1(b)). Hence, B^{-1} becomes zero, which decouples the moveouts in the CS and CR configurations. Accordingly, the parabolic common-offset response for diffractions reduces to

$$\begin{aligned} t_{\text{CO}}(\Delta\mathbf{x}_s, \Delta\mathbf{x}_g) = t_0^{\text{CO}} &+ \frac{\sin\alpha_s}{v_s}\Delta\mathbf{x}_s + \frac{1}{2}\frac{\cos^2\alpha_s}{v_s R_s}\Delta\mathbf{x}_s^2 \\ &+ \frac{\sin\alpha_g}{v_g}\Delta\mathbf{x}_g + \frac{1}{2}\frac{\cos^2\alpha_g}{v_g R_g}\Delta\mathbf{x}_g^2. \end{aligned} \tag{7}$$

Common-offset prediction for diffractions

Because of the decoupling of diffraction raypaths there is a strong redundancy of ZO and CO information for diffractions (Schwarz et al., 2014): the CS and CR responses in a common-offset measurement (see Figure 1(b)) are technically identical to two independent zero-offset measurements carried out at $\mathbf{x}_s$ and $\mathbf{x}_g$, as illustrated in Figure 1(c). Based on the assumption of reciprocity, which is valid for diffractions in an isotropic medium, comparing equations (4) and (7) leads to the following system of equations (assuming a correct choice of near-surface velocities):

$$\alpha_s = \alpha_0^s, \tag{8a}$$
$$\alpha_g = \alpha_0^g, \tag{8b}$$
$$R_s = R_{\text{NIP}}^s, \tag{8c}$$
$$R_g = R_{\text{NIP}}^g. \tag{8d}$$

The superscripts s and g indicate the ZO attributes measured at the source and receiver position, respectively (compare Figure 1(c)). This system of equations establishes the relations between ZO and CO diffraction attributes. Also the CO reference traveltime can be expressed by the two ZO reference traveltimes,

$$t_0^{\text{CO}} = \frac{t_0^{\text{ZO},s} + t_0^{\text{ZO},g}}{2}. \tag{9}$$

Relations (8) and (9) indicate the redundancy of ZO and CO information and thus allow the decomposition of any CO operator into two independent ZO operators at a source $\mathbf{x}_s$ and a receiver $\mathbf{x}_g$ (Schwarz et al., 2014),

$$t_{\text{CO}}(\mathbf{x}_s, \mathbf{x}_g, t_0^{\text{CO}}, \alpha_s, \alpha_g, R_s, R_g) = \frac{t_{\text{ZO}}(\mathbf{x}_s, t_0^{\text{ZO},s}, \alpha_0^s, R_{\text{NIP}}^s)}{2} + \frac{t_{\text{ZO}}(\mathbf{x}_g, t_0^{\text{ZO},g}, \alpha_0^g, R_{\text{NIP}}^g)}{2}. \tag{10}$$

This traveltime decomposition is exact for diffractions in isotropic media and thus may be called *common-offset prediction for diffractions*. Figure 2(b) displays an example of a stacking surface constructed using the traveltime decomposition method. Note that this decomposition principle only works for diffractions, because it is based on the assumption of decoupled up- and downgoing raypaths. In the reflection case, the previously introduced equations are not valid.

DIFFRACTION TRAVELTIME FIT

In order to confirm the redundancy of ZO and CO information, we carried out a diffraction traveltime fit on a simple synthetic model containing vertical and lateral heterogeneity by predicting CO traveltimes and attributes solely based on a ZO fit and comparing the results to the generic CO reference. The synthetic model consists of a plane interface at a depth of 300 m and a circular discontinuity with a radius of 5 km, whose top point lies at a depth of 400 m. The investigated diffractor is located at a depth of 1 km at a lateral position of 5 km. Figure 3 shows the model geometry and its velocities. The model and the reference traveltimes were generated with the NORSAR raytracing software. The traveltime fits were computed for each central source and receiver pair $(\mathbf{x}_s, \mathbf{x}_g)$ with MATLAB using a Nelder-Mead optimization scheme

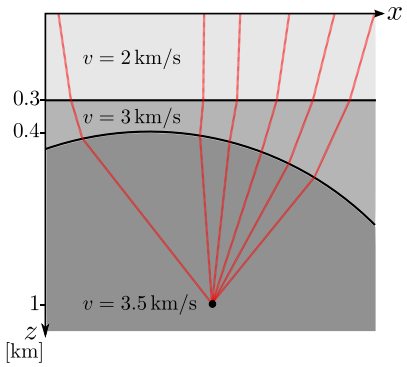

Figure 3: Geometry and velocities of the model used for the traveltime fit.

(Nelder and Mead, 1965) to find the best wavefield attributes, which minimize the traveltime error. All traveltimes within an aperture radius of 500 m from $(\mathbf{x}_s, \mathbf{x}_g)$ contributed to each fit. For the computation of traveltime surfaces in the ZO and CO domain the full parabolic traveltime formulations (2) and (6) were used.

Figures 4 and 5 show the obtained emergence angles and wavefront curvatures at the source for the CO prediction (left sides) and the generic CO fit (right sides). The respective receiver attributes are not displayed, because they contain the same features. Although it is only based on the results of a traveltime fit in the ZO section (accordingly, for $\mathbf{h} = 0$ the attributes coincide with the ZO input attributes α_0 and R_{NIP}), the CO prediction almost perfectly reproduces the attributes which were obtained from a generic CO fit. Only the wavefront curvatures show minimal deviations. The symmetry in the results clearly shows the expected redundancy of ZO and CO information for the diffraction case, which permits the prediction from ZO into CO.

The traveltime errors of CO prediction and generic CO fit are displayed in Figure 6. Additionally, the traveltime error obtained from CO extrapolation (which corresponds to partial CRS) is shown. As expected from the theory, the misfit of the CO prediction is identical to the one of the generic CO fit. This indicates that the introduced method is exact for diffractions: it is possible to predict the exact common-offset wavefield attributes from their zero-offset counterparts. The resulting error is merely produced by the inaccuracy of the second-order traveltime approximation. Also, a possible inexactness of the reference traveltimes might cause part of the error. A comparison of the CO prediction error to the misfit of the CO extrapolation, which is based on the same ZO input attributes, clearly reveals the advantages of the new method. Whereas the CO extrapolation rapidly loses accuracy in offset direction due to the global application of ZO operators, the magnitude of the CO prediction error does not increase with offset.

Due to the significantly smaller number of traveltime fits, the CO prediction only required 0.4 % of the CO reference computation time to produce the same results in this study. Note, however, that the most challenging task of the CO prediction, namely the identification of the two matching events at source and receiver, is missing in traveltime fitting.

IMPLEMENTATION

For the application to waveform data, we implemented the new CO prediction for diffractions into the well-known ZO CRS workflow (Mann, 2002). As input, the CO prediction requires the pre-stack data and results of the optimized ZO CRS stack, namely the optimized semblance and the attribute sections of the ZO wavefield attributes α_0 and R_{NIP}. In order to predict a CO trace for the half-offset $\mathbf{h}$ at the midpoint $\mathbf{x}_m$ the CO prediction requires as input two traces from the optimized ZO semblance section: The *imaginary source trace* at the location $\mathbf{x}_s = \mathbf{x}_m - \mathbf{h}$ on the CMP axis and the *imaginary receiver trace* at $\mathbf{x}_g = \mathbf{x}_m + \mathbf{h}$. Therefore, CO traces can be predicted only for values $\mathbf{h}$, which are multiples of the CMP spacing. On the two input semblance traces the two events which stem from the same diffractor have to be found. Different event combinations have to be tested in order to find the one which provides the best fit. For each sample t_0^s of the source trace $\mathbf{x}_s$ that contains an event the samples of the receiver trace are searched for the matching

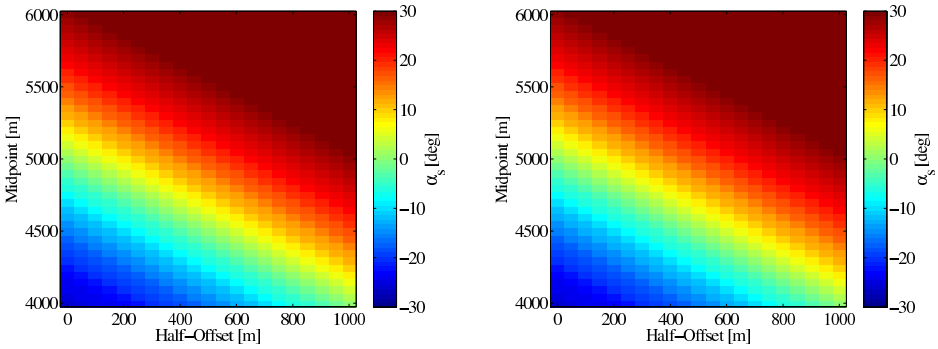

Figure 4: Emergence angles at the source α_s obtained from a) CO prediction and b) generic CO fit.

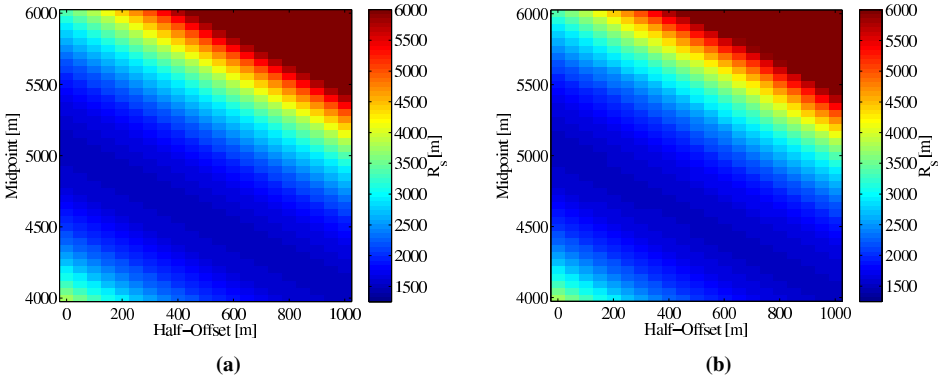

Figure 5: Wavefront curvatures at the source R_s obtained from a) CO prediction and b) generic CO fit.

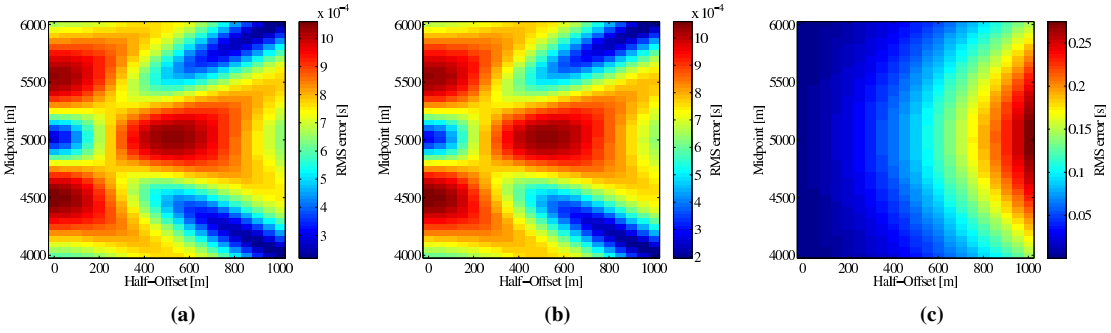

Figure 6: RMS errors of a) CO prediction and b) generic CO fit at the same scale. The traveltime error produced by CO extrapolation c) (plotted at a different scale) is much higher.

event. Assuming that for the traveltime difference between the two matching events the relation

$$\Delta t_0 \leq \frac{2\mathbf{h}}{v_0} \tag{11}$$

holds, the event search on the receiver trace can be confined. In order to be sure not to miss the matching event we doubled Δt_0 so that the samples of the receiver trace are searched within the interval $[t_0^s - 2\Delta t_0, t_0^s + 2\Delta t_0]$. At every sample t_0^g on the receiver trace, which contains an event, the new CO sample location t_0^{CO} is calculated using Equation (9) and the four common-offset wavefield attributes are extracted from the ZO attribute sections. They define the CO diffraction operator for $(\mathbf{x}_m, \mathbf{h}, t_0^{\mathrm{CO}})$. Of course, this method also allows results from event pairs, which do not belong to the same diffractor, to show up in the resulting CO section. However, this is no major problem, because due to the "wrong" stacking operator for non-matching events the resulting semblance and stack values will be very small even if the input semblance values are large. Note that the CMP axis of a predicted CO section for the half-offset $\mathbf{h}$ must be shortened by $\mathbf{h}$ at both ends, because in these areas do not exist attributes for source and receiver, respectively.

As output, the common-offset prediction provides the predicted CO stacks, the respective semblance and the four CO attribute sections for the pre-defined range of offsets. Note that the method is also applicable to zero-offset, where it might still serve to separate diffractions from reflections due to the use of a pure diffraction operator.

SIMPLE DATA EXAMPLE

In order to investigate the potential of the new method, we applied it to a simple waveform dataset based on the previously introduced model (see Figure 3). For this example, we included a second diffractor in a depth of 1.5 km at a lateral position of 3.5 km. The CO prediction results are compared to the respective results of the ZO-based partial CRS (Baykulov and Gajewski, 2009) and generic CO CRS (Zhang et al., 2001) processing. All results of the three methods for the common-offset 1000 m are displayed in Figure 7. They were computed with comparable processing parameters such as stacking apertures (see Bauer, 2014).

The results clearly reveal that the ZO operators, which are used for CO stacking in the partial CRS method, are not accurate anymore for large offsets. Both the stack and the semblance section computed by CO extrapolation appear blurred. In contrast to the extrapolation, the CO prediction results are of very high quality, because the method uses CO operators, which are, as deduced from the theory, exact for diffractions. Accordingly, the CO prediction does not lose accuracy with increasing offset. Note at this point that both methods are based on exactly the same input from ZO processing. The predicted CO stack (Figure 7(b)) reveals some artifacts, which are caused by wrong event combinations. In the respective semblance section (Figure 7(e)), small artifacts caused by the crossing of the two events are visible to its left and to its right. Therefore, they appear at a distance of 40 CMPs to the event crossing, which corresponds to the half-offset 500 m.

To the right of Figure 7 the generic CO CRS processing results are displayed. Whereas the stack looks very similar to the stack predicted using ZO information, the CO CRS semblance looks less smooth than its ZO-based counterpart, especially at the crossing of the two events. Additionally, the diffraction hyperbolae contain gaps to the left of their apices. These gaps, which do not appear in the stacked section, are not further investigated here, because the CO CRS results are merely provided as a reference for comparison.

In this simple waveform example, the two ZO-based methods partial CRS and CO prediction merely required 1.4 % and 1.5 % of the generic CO CRS computation time, respectively. Whereas partial CRS is always computationally efficient, the CO prediction was fast in this example because the dataset only contains few events. On complex data, however, the event search in its current implementation can make the method more expensive.

In conclusion, the processing results on the simple waveform dataset reveal the great potential of the new CO prediction for diffractions. As partial CRS (Baykulov and Gajewski, 2009), the CO prediction merely requires ZO wavefield attributes, but still it is able to provide results which for diffractions are of similar quality as the CO CRS reference. Being exact for diffractions in arbitrary isotropic media the method does, in contrast to the extrapolating partial CRS, not lose accuracy for larger offsets.

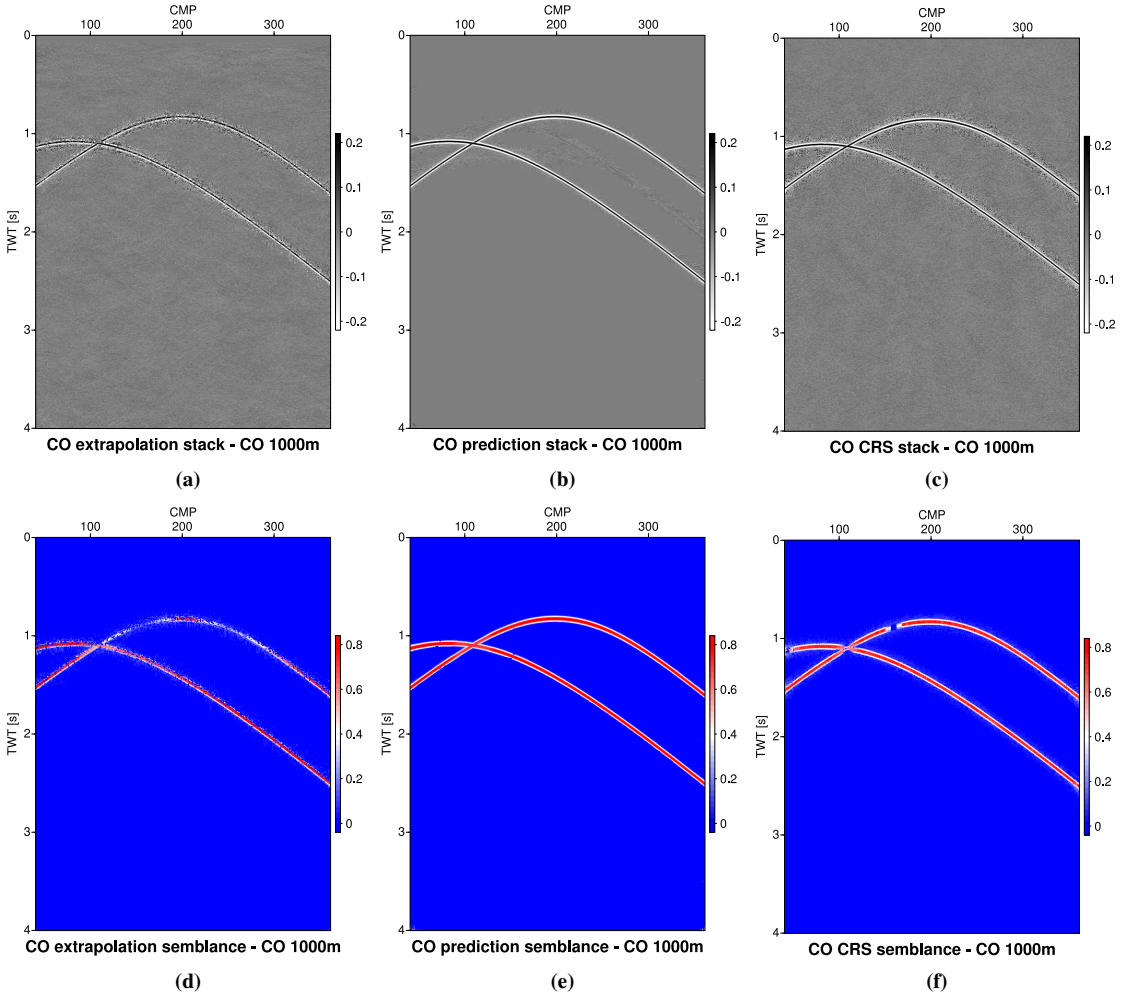

Figure 7: Partial CRS (left), CO prediction (center) and CO CRS (right) results of the simple waveform dataset for the offset 1000 m. In both stack (above) and semblance (below) the quality of the CO prediction results is equal to or even better than the generic CO CRS reference. The partial CRS results (left) show that the ZO operators are not accurate anymore for large offsets.

CONCLUSIONS AND OUTLOOK

We introduced a simple yet general decomposition principle for diffractions, which establishes a connection between zero-offset and common-offset diffraction wavefield information. In the diffraction case, move-outs in the common-shot and the common-receiver gather are decoupled, which allows the decomposition of each CO diffraction operator into two independent ZO operators. Thus, solely based on zero-offset CRS processing, this new method allows the prediction of exact common-offset diffraction wavefield attributes from their ZO counterparts.

A diffraction traveltime fit for a simple, heterogeneous model revealed the capability of the *CO prediction for diffractions* to fit traveltimes and estimate wavefield attributes of the same quality as a generic CO CRS fit (Zhang et al., 2001). Further, it demonstrated the distinct symmetries of diffraction wavefield attributes, which allow their prediction from ZO into CO. The exactness for diffractions distinguishes the new method from the ZO-based partial CRS approach (Baykulov and Gajewski, 2009), where ZO operators are used for CO stacking, which causes accuracy to decrease with offset.

Application of the new CO prediction for diffractions to simple waveform data revealed the method's ability to generate accurate CRS stacked sections for arbitrary common-offsets, which are of superior quality than respective results obtained from the ZO-based partial CRS (Baykulov and Gajewski, 2009) and of equal or even higher quality than generic CO CRS results (Zhang et al., 2001).

A next step is the application of the new method to complex synthetic data and to field data. The promising results of this application are presented in the second part of this report (Bauer et al., 2014).

ACKNOWLEDGMENTS

This work was kindly supported by the sponsors of the *Wave Inversion Technology (WIT) Consortium*, Karlsruhe, Germany. For the generation of reference traveltimes, the NORSAR-3D raytracing software was used. The traveltime fit was carried out with MATLAB.

REFERENCES

Bauer, A. (2014). From zero-offset to common-offset with diffractions. master's thesis, University of Hamburg.

Bauer, A., Schwarz, B., and Gajewski, D. (2014). From ZO to CO with diffractions: Complex data examples. *18th Annual WIT report*.

Baykulov, M. and Gajewski, D. (2009). Prestack seismic data enhancement with partial common-reflection-surface (CRS) stack. *Geophysics*, 74:V49–V58.

Bergler, S., Duveneck, E., Höcht, G., Zhang, Y., and Hubral, P. (2002). Common-reflection-surface stack for converted waves. *Stud. geophys. geod.*, 46:165–175.

Bortfeld, R. (1989). Geometrical ray theory: Rays and traveltimes in seismic systems (second-order approximations of the traveltimes). *Geophysics*, 54:342–349.

Hubral, P. (1983). Computing true amplitude reflections in a laterally inhomogeneous earth. *Geophysics*, 48:1051–1062.

Jäger, R., Mann, J., Höcht, G., and Hubral, P. (2001). Common-reflection-surface stack: Image and attributes. *Geophysics*, 66:97–109.

Mann, J. (2002). *Extensions and Applications of the Common-Reflection-Surface Stack Method*. PhD thesis, University of Karlsruhe.

Müller, T. (1999). *The Common Reflection Surface stack method – Seismic imaging without explicit knowledge of the velocity model*. PhD thesis, University of Karlsruhe.

Nelder, J. and Mead, R. (1965). A simplex method for function minimization. *American Mathematical Monthly*, 105:523–528.

Schwarz, B., Vanelle, C., and Gajewski, D. (2014). From zero-offset to common-offset with diffractions. In *76th EAGE Conference and Exhibition-Workshops*.

Spinner, M., Tomas, C., Marchetti, P., Gallo, C., and Arfeen, S. (2012). Common-offset CRS for advanced imaging in complex geological settings. *SEG Expanded Abstracts*, pages doi:10.1190/segam2012–1099.1.

Zhang, Y., Bergler, S., and Hubral, P. (2001). Common-reflection-surface (CRS) stack for common offset. *Geophysical Prospecting*, 49:709–718.